Comparison of the Global Structure and Dynamics of Native and Unmodified tRNA^{val}†

Annaleen Vermeulen,‡ Scott A. McCallum,§ and Arthur Pardi*

Department of Chemistry and Biochemistry, 215 UCB, University of Colorado, Boulder, Colorado 80309-0215

Received December 19, 2004; Revised Manuscript Received March 6, 2005

ABSTRACT: The effects of post-transcriptional modifications on the structure and dynamics of *Escherichia coli* tRNA^{val} were studied by NMR spectroscopy. NMR chemical shift data and residual dipolar couplings were used to show that the local secondary and tertiary structures are very similar in native and unmodified tRNA^{val}. Rigid body restrained molecular dynamics calculations showed that the global structure of tRNA is unchanged by the post-transcriptional modifications. Deuterium exchange NMR experiments were used to probe the dynamics and flexibility of native and unmodified tRNA^{val}. A similar set of slowly exchanging ($t_{1/2}$ > 3 min) imino protons were observed in both tRNAs, but the rates of exchange for the slowest exchanging imino protons were ∼20 times faster in unmodified than in native tRNA. These results demonstrate that the dynamics and flexibility of tRNA^{val}, but not the local or global structure, are significantly affected by post-transcriptional modifications.

tRNAs are the most highly post-transciptionally modified RNAs in the cell (*1*), and more than 80 different types of modifications have been identified (*2*). These modifications affect the shape, charge, hydrophobicity, and possible conformations of the individual nucleotides and have been shown to thermodynamically stabilize tRNAs (*3*, *4*). The diversity of these post-transcriptional modifications effectively increases the building blocks of RNA beyond the standard four nucleotides, thereby extending the capabilities of RNA to take on additional conformations and/or functions.

The anticodon loop in most tRNAs contains modified nucleotide(s) (Figure 1), and these modifications are important for optimal codon recognition (*5*). Modifications near the anticodon influence reading frame maintenance by affecting the stability of tRNA−mRNA complexes (*6*). Modified residues are also found near tertiary interactions where the D-loop and T-loop interact at the elbow of the L-shape (Figure 1). These modifications are thought to be important for stabilizing the correctly folded structures of tRNAs. Thermal denaturation studies of several *Escherichia coli* and yeast tRNAs show that the melting temperatures of native (fully modified) tRNAs are higher than those of unmodified tRNAs at both low and high Mg^{2+} concentrations (*7*−*11*). tRNAs from thermophiles also exhibit a higher percentage of modified residues (*12*). These results are consistent with the model in which the primary function of the modifications is to stabilize the folded structure of tRNA. This leads to the question of how post-transcriptional modifications affect the overall structure and dynamics of tRNA.

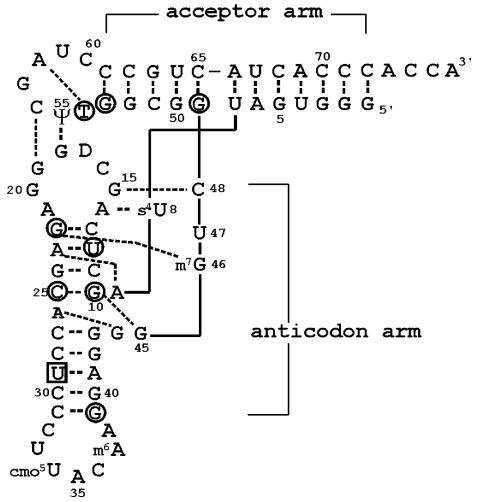

FIGURE 1: Secondary structure of native *E. coli* tRNA^{val}. Residues containing slowly exchanging imino protons observed in both native and unmodified *E. coli* tRNA^{val} are circled; the boxed residue indicates this imino proton was only observed to be slowly exchanging in unmodified *E. coli* tRNA^{val}.

Imino proton NMR data have been used to compare native and unmodified tRNAs. Hall et al. (*3*) first demonstrated that there were large differences in the imino spectra of native and unmodified yeast tRNA^{phe} in the absence of Mg^{2+}. They also showed that above 2 mM Mg^{2+}, the imino spectrum of unmodified yeast tRNA^{phe} had the same number of resonances, with unmodified bases having chemical shifts very similar to those of the native yeast tRNA^{phe}. Since imino proton resonances are observed for G and U residues involved in stable intramolecular hydrogen bonds, this

† This work was supported by NIH Grant AI 33098, and the NMR instrumentation was purchased with partial support from NIH Grant RR11969 and NSF Grant 9602941. We also thank the W. M. Keck Foundation for their generous support of RNA research on the Boulder campus.

* To whom correspondence should be addressed. Phone: (303) 492-6263. Fax: (303) 492-2439. E-mail: arthur.pardi@colorado.edu.

‡ Current address: Dharmacon Inc., 2650 Crescent Dr., Lafayette, CO 80026.

§ Current address: Department of Protein Engineering, Genetech Inc., South San Francisco, CA 94080.

10.1021/bi0473399 CCC: $30.25
Published on Web 03/31/2005

indicates that the base pairing and secondary structure of the native and unmodified tRNAs are similar at higher concentrations of Mg^{2+} (*3*). More recent NMR[1] studies of native and unmodified *E. coli* tRNA^{val} with a more complete set of imino proton resonance assignments concluded that the modifications help stabilize the tertiary interactions in the tRNA (*13*). However, the modifications are not required for some of the biological functions of tRNA. For example, in vitro experiments show the kinetics of aminoacylation of unmodified tRNA^{phe} are similar to those of native tRNA^{phe} in the presence of high levels of Mg^{2+} (10 mM) (*3*). These results suggest that native and unmodified tRNAs have similar biological activity as long as enough Mg^{2+} is present to compensate for the lack of post-transcriptional modifications.

The X-ray crystal structures of several free native tRNAs have been determined, but to date, there are no crystal structures for free, unmodified tRNAs. These tRNA structures all adopt the characteristic L-shape global fold, but there is some variation in the global conformation. The angles between the acceptor and anticodon arms in the crystal structure of free yeast tRNA^{phe}, tRNA^{asp} and initiator tRNA^{fmet}, and human tRNA^{lys} vary from 76 to 96° (*14*−*18*). This raises the question of whether tRNAs adopt different conformations in solution and how the post-transcriptional modifications affect the global conformation of individual tRNAs. Transient electric birefringence measurements showed an interarm angle of 80−90° for unmodified yeast tRNA^{phe} (*19*, *20*), which is consistent with the 86° interarm angle of the yeast tRNA^{phe} crystal structure. These experiments require long (75 bp) extensions of the helical arms and thus are not readily applied to native tRNAs. Traditional NMR methods that employ short-range proton−proton distance and torsion angle constraints can be used to generate high-resolution local structure but are not able to determine the global structure of extended molecules such as nucleic acid double helices (*21*). However, improved methods for partially ordering macromolecules in solution have made it possible to routinely measure RDCs. Since the RDCs depend on both the distance and relative orientation of the nuclei in the magnetic field, these data allow distant parts of macromolecules to be positioned relative to each other (*22*−*25*). Several domain orientation techniques have been used to determine the global structures of macromolecules from RDCs (*26*−*32*). RDC data and domain orientation techniques were used here to compare the global structures of modified and unmodified *E. coli* tRNA^{val}.

Post-transcriptional modifications have been shown to affect the thermodynamic stability of tRNA (*8*, *9*, *13*); thus, it follows that they will also affect the dynamics and flexibility of tRNAs. The kinetics for solvent exchange of imino and amino protons can be used to probe the dynamics of nucleic acids (*33*, *34*). These solvent exchange rates are influenced by hydrogen bonding and base pair opening of the secondary and tertiary structures. The imino protons in standard double-helical regions have relatively fast solvent exchange kinetics (0.1−10 s^{-1} at 25 °C), but very slowly exchanging imino protons have been observed for post-transcriptionally modified tRNAs with half-lives as long as several days (*34*−*37*). However, the effect of modifications on the exchange kinetics has not been determined. In this work, the deuterium exchange kinetics for native and unmodified *E. coli* tRNA^{val} are compared in an effort to better understand how the dynamics of *E. coli* tRNA^{val} are affected by post-transcriptional modifications. The NMR and deuterium exchange studies performed here demonstrate that modifications lead to significant changes in dynamics, but not the local or global structure of tRNA^{val} in solution.

EXPERIMENTAL PROCEDURES

Sample Preparation. Native (fully modified) *E. coli* tRNA^{val} was prepared by overexpression in *E. coli* containing the pVALT7 plasmid (*7*). For ^{15}N-labeled native tRNA^{val}, a 100 mL overnight culture was used to inoculate 1 L of minimal medium containing $^{15}NH_4Cl$ as the only nitrogen source, and the native tRNA^{val} was purified as previously described (*7*, *38*, *39*). Unmodified tRNA^{val} was prepared by in vitro transcription from plasmid DNA templates as described previously (*3*, *13*). The tRNAs were exchanged into NMR buffer [10 mM sodium phosphate (pH 7.0), 80 mM NaCl, 5 mM $MgCl_2$, and 0.1 mM EDTA] in a 90% H_2O/10% D_2O mixture by extensive buffer exchange using Centricon YM-10 centrifugal filter devices (Millipore, Bedford, MA). An alignment medium of polyoxyethylene-5-octyl ether and 1-octanol (*40*) was prepared by adding 35 μL of C8E5 to 1 mL of a 90% H_2O/10% D_2O mixture, and then up to 14 μL of 1-octanol was added dropwise until the solution became opalescent, indicating formation of the liquid crystal phase. This alignment medium was then added to a lyophilized sample, yielding 1 mM native tRNA^{val}. Pf1 filamentous phage was prepared as previously described (*41*), and unmodified tRNA^{val} in a 90% H_2O/10% D_2O NMR buffer was added to the concentrated Pf1 to give a sample of 0.3 mM tRNA in 15 mg/mL Pf1. The quadrupole splitting of the ^2H_2O resonance was used to quantify the degree of alignment of these tRNA samples (*41*).

NMR Data Collection. NMR experiments were performed on Varian Inova 500 or 600 MHz spectrometers with triple-resonance probes and *z*-axis pulsed-field gradients. The NMR data were processed using FELIX97 (Molecular Simulations Inc., San Diego, CA). 1D ^1H spectra were collected using a jump−return pulse sequence for water suppression (*42*). 2D $^1H-^1H$ NOESY and $^1H-^{15}N$ HSQC experiments (*43*, *44*) were used to confirm the resonance assignments of native and unmodified *E. coli* tRNA^{val} imino protons (*28*, *39*, *45*). Doublet-separated sensitivity-enhanced 2D $^1H-^{15}N$ HSQC experiments were used to measure one-bond $^1H-^{15}N$ couplings in the isotropic and aligned tRNA samples (*46*). The RDCs were obtained by subtracting the $^1H-^{15}N$ couplings measured in the aligned and isotropic samples (Table 1). The experimental details for the NMR experiments are given in the Supporting Information.

[1] Abbreviations: 1D, one-dimensional; 2D, two-dimensional; HSQC, heteronuclear single-quantum correlation spectroscopy; C8E5, polyoxyethylene-5-octyl ether; NMR, nuclear magnetic resonance; NOESY, two-dimensional nuclear Overhauser effect spectroscopy; RDCs, residual dipolar couplings; EDTA, ethylenediaminetetraacetate; s^4U, 4-thiouridine; D, dihydrouridine; cmo^5U, uridine 5-oxyacetic acid; m^6A, N^6-methyladenosine; m^7G, 7-methylguanosine; T, 5-methyluridine; Ψ, pseudouridine.

Table 1: Normalized Residual Dipolar Couplings for the Base-Paired Imino NH Groups of *E. coli* tRNA^{val} [a]

native tRNA^{val} [b]		unmodified tRNA^{val} [c]	
residue	RDC (Hz)	residue	RDC (Hz)
G1	*−11.3*	*G1*	*−11.7*
G2	*10.0*	*G2*	*10.2*
G3	*14.2*	*G3*	*13.5*
U4	*4.0*	*U4*	*6.0*
G5	*−24.2*	*G5*	*−26.0*
U7	*−5.0*	*U7*	*−10.9*
s^{4}U8	**−1.0**	**U8**	**−2.0**
G10	−20.9	G10	−13.5
U12	−3.7	U12	2.0
G15	**−31.0**	**G15**	**−30.1**
G18	**−18.6**	**G18**	**−21.1**
G22	−8.5	G22	2.4
G24	−11.4	G24	−13.3
U29	−26.5	U29	−28.4
G39	−16.6	G39	−21.6
G40	−30.7	G40	−30.1
G42	−9.9	G42	−10.4
m^{7}G46	**−25.0**	**G46**	**−26.5**
G49	*28.1*	*G49*	*31.4*
G50	*25.3*	*G50*	*21.5*
G52	*−23.8*	*G52*	*−29.4*
G53	*0.1*	*G53*	*−16.7*
T54	**7.6**	**U54**	**3.1**
Ψ55N3	**20.9**	**U55**	**20.6**
G63	*3.0*	*G63*	*2.6*
U64	*30.1*	*U64*	*26.0*
U67	*−19.9*	*U67*	*−24.5*

[a] The estimated experimental error is ±1.5 Hz. The RDCs for the acceptor arm are in italic type; the RDCs for the anticodon arm are in plain type, and the RDCs for the tertiary interactions are in boldface type. [b] Sample conditions are as follows: 10 mM sodium phosphate (pH 7.0), 80 mM NaCl, 5 mM $MgCl_2$, and 0.1 mM EDTA at 15 °C. [c] Sample conditions are as follows: 10 mM sodium phosphate (pH 7.0), 80 mM NaCl, 5 mM $MgCl_2$, and 0.1 mM EDTA at 25 °C. These RDCs were normalized by multiplying them by 1.625 to account for different degrees of alignment between the native and unmodified tRNA samples.

Rigid Body Structure Calculations with RDCs. Residual dipolar coupling can be described by the following equation (*22*, *47*):

$$D_{PQ} = D_a[(3\cos^2\theta - 1) + {}^3/_2 R(\sin^2\theta \cos 2\phi)] \quad (1)$$

where D_{PQ} is the residual dipolar coupling between nuclei P and Q, D_a is a function of the degree of alignment of the molecule, as well as the gyromagnetic ratio, internuclear distance, and generalized order parameter (S) of nuclei P and Q, R is the rhombicity, and θ and ϕ define the orientation of the internuclear vector PQ in spherical coordinates.

A modified version of X-PLOR version 3.21 that employs a square-well potential for residual dipolar couplings was used for structure calculations (*48*, *49*). The helical arms in the tRNA were modeled as A-form structures as previously described (*28*), and the arm orientation calculation treats the acceptor and anticodon arms as rigid helices while reorienting the arms to give the best fit to the RDCs. A set of 50 calculations was performed starting with random orientations of the arms and included the ^{1}H−^{15}N imino RDCs with errors of ±1.5 Hz. D_a and R were determined in X-PLOR using a rigid body fit with a grid search procedure (*47*) with the details of the rigid body arm orientation calculations given elsewhere (*38*).

Computer Simulations for Error Determination in Arm Orientation Calculations. A computer simulation was performed to determine how variations in the local structure (structural noise) (*50*) affect the results of the arm orientation calculation. The A-form model structure of unmodified tRNA^{val} (*28*) was used as the target structure, and a set of perfectly accurate imino proton RDCs that correspond to the experimental data were generated with D_a and R values of −17 Hz and 0.65, respectively.

To simulate structural noise, a FORTRAN program was written that generates starting structures that have systematic errors in the orientations of the ^{15}N−^{1}H internuclear vectors of imino bonds. Structural noise was introduced into the target structure by changing the orientation of the imino group internuclear vector by sampling a distribution of orientations within a cone (see Figure S1 of the Supporting Information). Fifty starting structures were generated with structural noise of 0, 2.5, 5, 7, 10, or 20°, and domain orientation calculations were performed for each of these data sets. The correct alignment magnitude and rhombicity for the target structure ($D_a = -17$ Hz and $R = 0.65$) were used in these calculations. A calculation was also performed where in addition to the imino bond ^{1}H−^{15}N RDCs, ^{1}H−^{13}C RDCs were simulated for all the C1′H1′ groups in the helical arms using a structural noise of 7°.

Calculations of Interarm Bend and Twist Angles. CURVES version 5.1 (*51*) was used to determine the average helical axis of the acceptor and anticodon arms for the tRNA structures. An in-house FORTRAN program was used to calculate the interdomain bend and twist angles for these helical axes.

Deuterium Exchange Experiments. A 1 mL bed volume G-25 size exclusion spin column was equilibrated with NMR buffer in 99% D_2O (on ice), and the native or unmodified *E. coli* tRNA^{val} in a 90% H_2O/10% D_2O mixture (2.7−4 mM tRNA in a volume of 150 μL) was applied to the column. tRNA was eluted by centrifuging for 2 min at 1500*g*. The sample was immediately diluted with 99% D_2O NMR buffer to 400 μL and transferred to a Shigemi NMR tube, and the first ^{1}H 1D experiment was completed 4 min after the sample was applied to the column. The intensities of the slowly exchanging peaks were measured using FELIX97 and were fit to the simple exponential decay $I = I_o(e^{-kt}) + c$ in Kaleidagraph 3.5 (Synergy Software), where I is the intensity of the peak at time t, I_o is intensity of the peak at time zero, k is the rate constant [$t_{1/2} = \ln(2)/k$], and c is a constant to correct for baseline offset and/or residual H_2O in the sample.

RESULTS

Characterizing Native and Unmodified tRNA^{val}. Comparison of the ^{1}H−^{15}N HSQC spectra of native and unmodified tRNA^{val} shows the same number of cross-peaks in the imino region (Figure 2), indicating a similar number of hydrogen bonding interactions for imino protons in both these tRNAs. As seen in Figure 2, five imino groups show significant chemical shift differences between these two tRNAs, and four of these are the modified bases, s^{4}U8, T54, m^{7}G46, and Ψ55. Although G18 is not modified, it also has a small change in ^{1}H chemical shift, which may arise from G18 base pairing to Ψ55 and being directly adjacent to D17 and near T54. Overall, comparison of the ^{1}H and ^{15}N chemical shifts

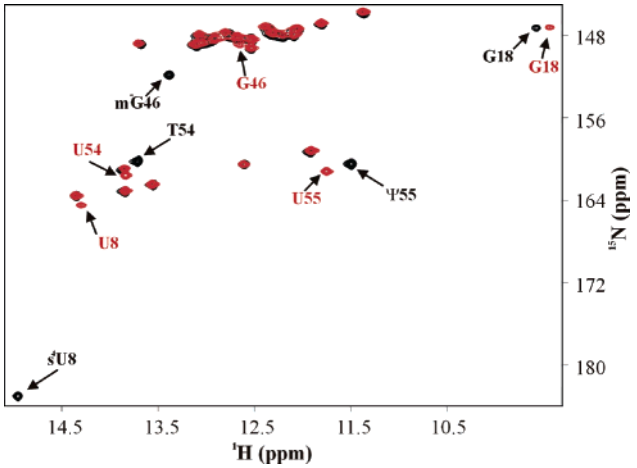

FIGURE 2: Imino region of the 2D $^{1}H-^{15}N$ HSQC spectra of native (red) and unmodified (black) *E. coli* tRNA^{val} in 5 mM Mg^{2+} at 25 °C. Arrows indicate residues that show a change in ^{1}H chemical shift of >0.2 ppm.

is consistent with nearly equivalent local, hydrogen bonding structures of native and unmodified tRNA^{val} in 5 mM Mg^{2+}.

Residual Dipolar Couplings of Native and Unmodified tRNA^{val} Structures. The RDCs were measured here for both native and unmodified tRNA^{val}. The results for the native tRNA in C8E5 alignment medium were identical to those previously published under slightly lower salt conditions with Pf1 alignment medium (*28*), and comparison of RDC data in a variety of different alignment media shows that the alignment tensors and normalized RDCs for native tRNA^{val} are the same in all the alignment media that were tested (unpublished results). A plot of the normalized $^{1}H-^{15}N$ RDCs of native and unmodified tRNA^{val} shows that, except for residues 10, 22, and 53, all the RDCs are similar (all others have differences of less than 6 Hz) (Figure 3). This indicates that the imino bond vector orientations for most residues are very similar in both tRNAs.

Global Structure Determinations of Native and Unmodified tRNA^{val} from Residual Dipolar Couplings. We previously used RDCs and the domain reorientation-type program CONFORMIST to determine the orientation of the helical arms for native tRNA^{val} (*28*). A slightly modified procedure

Table 2: Summary of Alignment Tensor Information for Rigid Body Restrained Molecular Dynamics Calculations of tRNAs[a]

	D_a (Hz)	R	rmsd[b] (Hz)
native tRNA^{val}			
acceptor arm[c]	15.5	0.60	4.63
anticodon arm[d]	23.5	0.30	5.35
rigid body arm orientation[e]	17.0	0.55	5.56
unmodified tRNA^{val}			
acceptor arm[c]	10.5	0.65	1.43
anticodon arm[d]	12.5	0.50	2.65
rigid body arm orientation[e]	12.5	0.50	2.63

[a] The errors in D_a and R are approximately ±1 Hz and ±0.1, respectively. [b] Root-mean-square deviation from measured RDCs to RDCs predicted from the structure as determined by X-PLOR. [c] Grid search results from a rigid body fit of data to the A-form model with only acceptor arm RDCs. [d] Grid search results from a rigid body fit of data to the A-form model with only anticodon arm RDCs. [e] Grid search results from full arm orientation structure calculation with all arm RDCs.

is employed here where the restrained molecular dynamics package, XPLOR, was used to determine the orientation of the helical domains while simultaneously producing a structure consistent with standard covalent, bond angle, steric, and experimental constraints. XPLOR requires input of alignment tensor values D_a and R, and a grid search refinement method was used to determine the alignment tensor (*25*, *47*). The first step in determining the global orientation of a molecule by RDCs is demonstrating that the individual domains orient as a single rigid species. Thus, independent grid search refinements were performed using RDC data for only the acceptor or anticodon arm in each of the tRNAs. The results are given in Table 2 and show similar values for D_a and R for the acceptor and anticodon arms, confirming that each tRNA is orienting as a rigid species.

Rigid body restrained molecular dynamics calculations were employed to determine the arm orientation in these tRNAs. This calculation involves three stages: (i) randomization of the orientation of the anticodon arm relative to the acceptor arm, (ii) rigid body restrained molecular dynamics and simulated annealing refinements to reorient the anticodon arm relative to the acceptor arm by simultaneously determining the best fit of the alignment tensor to the RDCs in a grid search of D_a and R, and (iii) energy

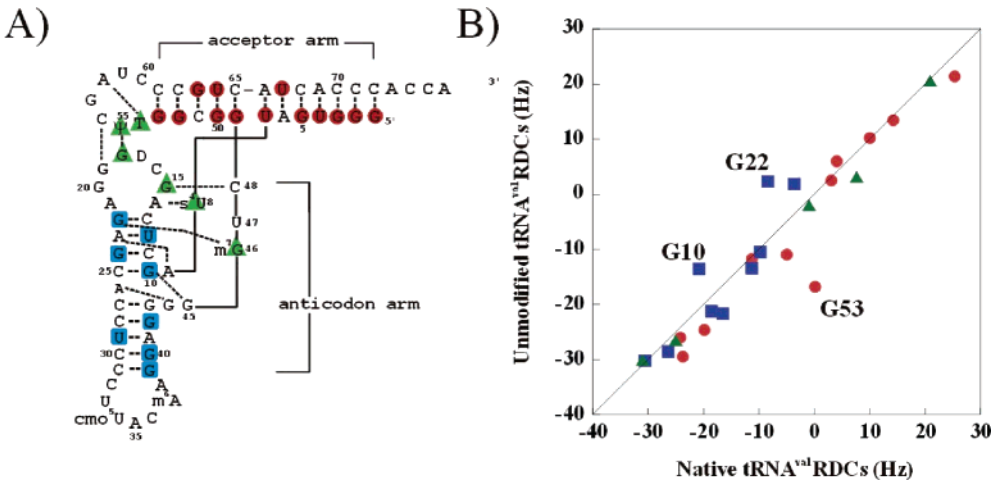

FIGURE 3: Normalized RDCs for native *E. coli* tRNA^{val} at 15 °C and unmodified *E. coli* tRNA^{val} at 25 °C (the unmodified RDCs were normalized to account for the different degree of alignment in the two samples). Positions of RDCs in the secondary structure are color-coded for the acceptor arm (red), the anticodon arm (blue), and the tertiary contact (green), and the residues with the largest differences are labeled.

Table 3: Simulations of RDC Data with Different Degrees of Structural Noise[a]

structural noise (deg)[b]	RDC rmsd (Hz)	interarm angle (deg)	twist angle (deg)
0		85.8	177.4
2	1.1 ± 0.2	86 ± 6	177 ± 2.9
5	2.4 ± 0.5	87 ± 6	178 ± 4.2
7	3.1 ± 0.8	87 ± 9	177 ± 5.1
10	4.3 ± 1.1	91 ± 10	178 ± 6.9
20	7.9 ± 1.9	87 ± 20	176 ± 14
7[c]	3.4 ± 0.5	86 ± 4	177 ± 3.3

[a] Arm orientation calculations using perfectly accurate imino $^{1}H-^{15}N$ RDC data (with a precision of ±1.5 Hz) and also including various degrees of structural noise. Each set of calculations was performed for 50 different starting structures, and the results are for the average of all 50 structures. [b] The cone angle of the internuclear vector used for simulating structural noise in starting structures (see Figure S1 of the Supporting Information). [c] In addition to the imino RDC data, these calculations also included $^{1}H-^{13}C$ C1′−H1′ RDCs. Structural noise was also included for the C1′−H1′ internuclear vector.

minimization to ensure satisfactory covalent structure (see Experimental Procedures).

These arm orientation calculations show that native tRNA^{val} has average interarm and twist angles of 103 ± 1° and 179 ± 1°, respectively (for a set of 50 structures). These angles are identical to previous results for this system (*28*). The results for the unmodified tRNA^{val} are within error of these for the native tRNA (interarm and twist angles of 100 ± 1° and 177 ± 1°, respectively), providing further evidence that the global conformation of the tRNA^{val} is unchanged by the post-transcriptional modifications. As discussed below, these errors only account for uncertainty in the measured RDCs and likely underestimate the true error of the calculated interarm and twist angles.

Computer simulations were next performed to estimate how variations in the local orientation of $^{1}H-^{15}N$ imino groups affect the interarm angles in tRNA. A model structure for native tRNA^{val} (*28*) was used as the target structure. To mimic the experimental data, a perfectly accurate set of 21 RDCs was calculated from the target structure and the RDCs were input with the same precision (±1.5 Hz) as the experimental data. These RDCs were then used as input for five separate arm orientation calculations, which differ in the amount of structural noise introduced for the H−N vectors (Table 3).

The results showed that for a structural noise of 2°, the interarm angle has a standard deviation of ±6°. When the structural noise increases to 10 or 20°, the standard deviation in the interarm angle is ±10 or ±20°, respectively. Similarly, for a structural noise of 2°, the twist angle standard deviation is ±2.9° and increases to ±14° for a structural noise of 20°. The rmsds of the RDCs increase from 1.1 to 7.9 Hz when structural noise increases from 2 to 20°.

To determine how additional RDCs improve the arm orientation calculations, 64 $^{1}H-^{13}C$ RDCs for sugar C1′H1′ groups in the helical arms were added to the calculation. This new set of RDCs was used to perform arm orientation calculations with starting structures that contain a structural noise of 7°. As expected, the additional RDCs reduce the interarm angle error from 9 to 4° and improve the twist angle error from 5.1 to 3.3° (Table 3). These data suggest that the accuracy of the local structure is very important when only a small set of RDCs is used to orient different domains.

Table 4: Hydrogen Exchange Kinetics for Native and Unmodified *E. coli* tRNA^{val} [a]

	resonance (ppm)	assignment(s)	$t_{1/2}$ (min)
native	13.87	U12 H3	33 ± 2
	13.69	G24 H1/T54 H3[b]	1500 ± 350
	13.02	G22 H1	108 ± 10
	12.99	G53 H1	125 ± 10
	12.47	G10 H1/G39 H1	15 ± 2
	12.04	G49 H1	14 ± 2
unmodified	13.87	U12/U54/U29 H3[b]	73 ± 20
	13.71	G24 H1	56 ± 20
	13.05	G53 H1	~3−5
	12.89	G22 H1	~3−5
	12.47	G10 H1/G39 H1[b]	~3−5
	12.05	G49 H1	~3−5

[a] Deuterium exchange experiments were performed in 10 mM sodium phosphate (pH 7.0), 80 mM NaCl, 5 mM $MgCl_2$, and 0.1 mM EDTA at 5 °C. Errors in $t_{1/2}$ were estimated from the standard deviation of two measurements and the curve fit of the data. [b] Overlapped resonances with the underlined residues showing the most likely assignment of the slowly exchanging proton.

Deuterium Exchange of tRNA. 1D proton−deuterium exchange experiments were used to compare base pair dynamics in native and unmodified tRNA^{val}. Six slowly exchanging resonances were observed in native tRNA^{val} with half-lives from 14 to 1500 min (Table 4), and four resonances were unambiguously assigned (U12, G22, G53, and G49). The slowly exchanging resonance at 13.69 ppm is assigned to the imino proton of either G24 or T54, and the resonance at 12.47 ppm is the imino proton for either G10 or G39, with G10 being the most likely since it is slowly exchanging in native yeast tRNA^{phe} (*35*). For unmodified tRNA^{val}, two resonances exhibited very slow exchange with half-lives of 56 and 73 min. Four other resonances had not fully exchanged by the first time point (4 min), but their exchange was so near the detection limit of this method that half-lives could not be confidently determined. The resonance with a half-life of 73 min is overlapped and is from the imino proton(s) of U12, U54, and/or U29. The peak with the next longest half-life (56 min) is unambiguously assigned to G24. Three of the four resonances with lifetimes of <5 min were unambiguously assigned, and the other one is the imino proton of either G10 or G39. Summaries of the exchange kinetics for slowly exchanging imino protons in native and unmodified tRNA^{val} are given in Table 4.

DISCUSSION

tRNAs have the highest level of post-transcriptional modifications of any known RNAs, and a significant percentage of the genes in a bacterial cell are dedicated to tRNA-modifying enzymes (*4*). Thus, it is expected that these modifications are critical for tRNA function. Some modifications are thought to be important for stabilizing the folded structure of tRNA, and others are important for molecular recognition. For example, under physiological conditions, the rates of aminoacylation of unmodified tRNAs are much slower than for native tRNAs. However, with high levels of Mg^{2+}, these rates are similar for the modified and unmodified species (*8*). It is thought that the post-transcriptional modifications indirectly affect how the tRNAs are recognized by the aminoacylation enzymes by affecting the conformation or dynamics of the tRNA.

Modifications in the anticodon region of tRNAs help ensure proper codon recognition in the ribosome and

influence reading frame maintenance by affecting the stability of tRNA−mRNA complexes (*5*). Modified residues are also found near tertiary interactions where the D-loop and T-loop interact in tRNA (Figure 1). These modifications are thought to help thermodynamically stabilize the tRNAs, and thermal denaturation studies of several *E. coli* and yeast tRNAs have shown that the melting temperatures of native tRNAs are higher than those of unmodified tRNA at both low and high Mg^{2+} concentrations (*7*−*11*). For bacterial systems, the extent of modifications of tRNA increases significantly in thermophiles compared to mesophiles (*12*). These results indicate that the degree of post-transcriptional modification helps stabilize the correctly folded structure of tRNA in cells.

Local Structure Probes of Modified and Unmodified tRNA^{val}. NMR studies of the imino protons have previously been used to compare native and unmodified tRNAs. Hall et al. first demonstrated that in the absence of Mg^{2+}, there are large differences in the imino proton spectra of native and unmodified yeast tRNA^{phe}. However, above 2 mM Mg^{2+}, the imino proton data indicate that the base pairs and base triples are similarly formed in the native and unmodified structure (*3*). A more recent imino proton NMR investigation with more complete resonance assignments for native and unmodified *E. coli* tRNA^{val} showed that many of the tertiary interactions observed in modified tRNA^{val} did not form in the unmodified tRNA^{val} with no Mg^{2+}. However, in 5 mM Mg^{2+}, the imino proton spectra of the modified and unmodified tRNA^{val} are quite similar. From this study, it was concluded that modifications stabilize the tertiary structure in the absence of Mg^{2+} (*13*). The additional ^{15}N chemical shift data obtained here confirm these previous studies, where both the ^{1}H and ^{15}N chemical shifts for imino groups are very similar, indicating comparable hydrogen bonding interactions in modified and unmodified tRNA^{val}.

RDCs are a sensitive function of orientation and distance and, therefore, represent a valuable probe of the local and global structure of macromolecules (*25*, *47*). The vast majority (24 of 27) of the normalized $^{1}H-^{15}N$ RDCs for imino groups of native and unmodified tRNA^{val} have similar values, demonstrating that these N−H bonds have similar orientations in both molecules (Table 1 and Figure 3). Interestingly, the normalized RDCs for residues 8, 46, 54, and 55 are also very similar, even though these residues contain post-transcriptional modifications in native tRNA^{val}. The largest difference in RDCs is G53; this base is adjacent to a T in native tRNA^{val} and a U in unmodified tRNA^{val}, and there may be slightly different stacking to accommodate the additional methyl group. The RDCs for G22 are also significantly different, but this base forms a triple with m^7-G46 in native tRNA^{val}; thus, the additional methyl group on residue 46 in native tRNA^{val} may affect the orientation of G22 in the base triple. G10 is not close to any modified residues, yet shows a difference of more than 7 Hz in the RDCs. This difference indicates an alternate orientation or dynamics for G10 in the two tRNAs, but the origin of the difference in RDC is not clear. Overall, comparison of the RDCs demonstrates that the unmodified and native tRNA^{val} have similar local (and global) structures.

Plotting the $^{1}H-^{15}N$ imino RDCs as a function of position in the secondary structure for both native and unmodified tRNA^{val} shows the presence of a sinusoidal wave type pattern for the acceptor arm (see Figure S2 of the Supporting Information). This type of dipolar wave has been used to identify regular helical structures in peptides and RNAs (*52*, *53*) and indicates that the coaxially stacked T-stem and acceptor stem form a continuous A-form helix. There is no obvious periodicity in the plot for the anticodon arm. The anticodon arm is composed of the anticodon stem coaxially stacked on the D-stem. The D-stem is involved in base triples and tertiary interactions that may cause the positions of the nucleotides to deviate somewhat from a regular A-form helix conformation. The plots for native and unmodified tRNA^{val} are very similar, indicating that post-transcriptional modifications do not change the general helical structure of the tRNAs.

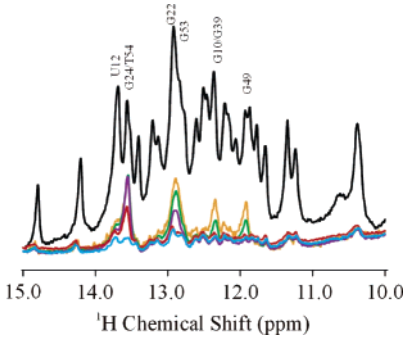

FIGURE 4: Deuterium exchange monitored by imino proton NMR spectra of native *E. coli* tRNA^{val} at 5 °C. The reference spectrum in a 10% D_2O/90% H_2O mixture is shown on top, and the colored spectra were recorded different times after exchange into D_2O (orange, 5 min; green, 24 min; purple, 108 min; red, 31 h; and cyan, 140 h). The reference spectrum was acquired with more scans than the other spectra (256 vs 32).

Global Structure of Native and Unmodified tRNA^{val}. Comparison of the RDCs for modified and unmodified tRNA^{val} (Figure 3B) indicates that these tRNAs have qualitatively similar global structures. The rigid body restrained molecular dynamics calculations confirm this conclusion, where both native and unmodified tRNA^{val} have interarm bend and twist angles of approximately 103 ± 1° and 179 ± 1°, respectively (Figure 5). However, these calculations likely underestimate the true error in determining these angles. A variety of factors will contribute to errors in final global structures, including uncertainty in measurements of RDCs, variation in local or global dynamics that lead to differences in the order parameter (S), uncertainties in estimating the D_a and R values of the alignment tensor, and structural noise arising from incorrect local structure for the individual domains. We employed a conservative error in the RDCs (±1.5 Hz) which helps account for slight variations in the order parameters S for individual imino groups. However, even this conservative error leads to only a very small error (±1°) in the orientation of the domains.

To more thoroughly address how other factors affect the precision of the final global structures, several types of calculations were performed using experimental or simulated data for native tRNA^{val}. Calculations were performed using the experimental data for native tRNA^{val}, where D_a was varied from 15.0 to 19.0 Hz. As seen in the Supporting Information (Table S2), this results in interarm bend angles ranging from 101 to 106° but no change in the interarm twist. For calculations where the rhombicity was varied from 0.4 to 0.65, the interarm bend angle ranged from 99 to 107° and the twist angle ranged from 181 to 177°. Thus,

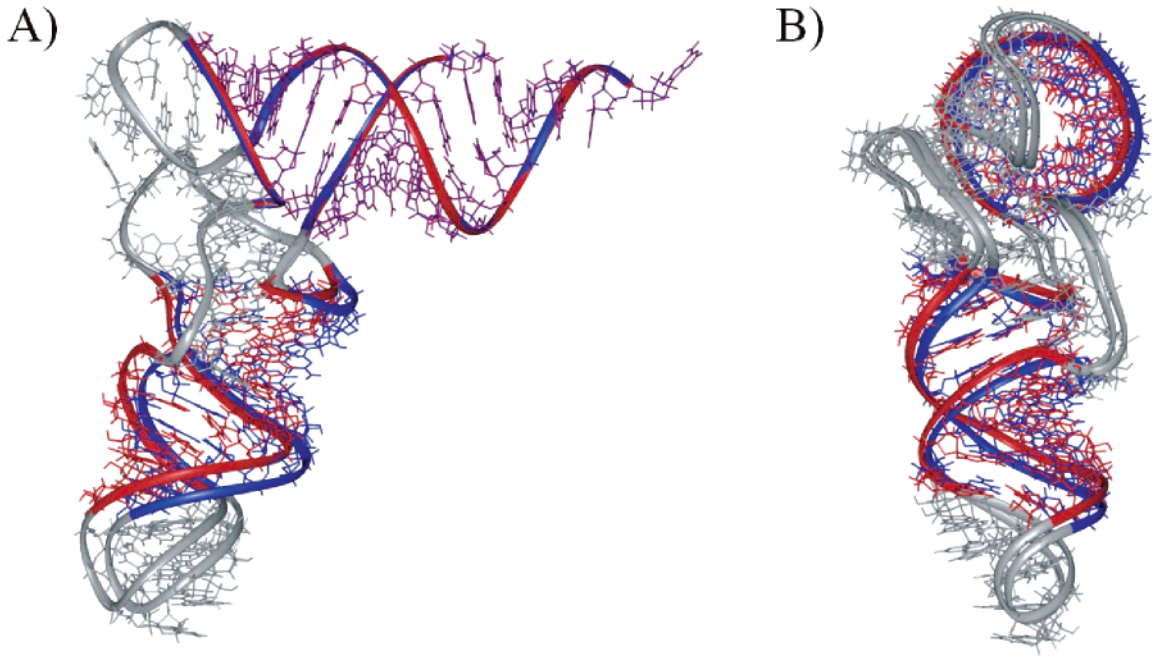

FIGURE 5: Relative orientations of the acceptor and anticodon arms of native (blue) and unmodified (red) *E. coli* $tRNA^{val}$ when five structures from the rigid body domain reorientation calculations are superimposed on the acceptor arm. (A) A view illustrating the characteristic L-shape and (B) rotated 90° to give a view down the acceptor arm from the loop end. The interarm angles for native and unmodified *E. coli* $tRNA^{val}$ are 103 and 100°, respectively, and the twist angles are 179 and 177°, respectively. The uncertainty in interarm angle depicted here (±1°) is for fitting of the RDCs, but as discussed in the text, a more realistic uncertainty including structural noise arising from local structural variations is ~10°.

uncertainty in the alignment tensor magnitudes leads to a larger variation in the orientation of the helical arms of tRNA than uncertainty in the measured RDCs. Next, simulations were performed to mimic inaccuracies in the local structure of the individual domains being oriented in these rigid body calculations. Structural noise as small as 2° results in an interarm bend angle error of ~6° (Table 3). Thus, the introduction of structural noise has a much larger affect on the precision of the arm orientation than errors in RDCs, D_a, or R. The simulations show that with the limited set of RDCs used here, small differences (<5°) in the arm orientation between native and unmodified tRNA could not be confidently determined. These simulations also showed that errors in arm orientation can be significantly reduced by including additional RDCs, such as H1′−CH1′ (see Table 3).

The simulations made it possible to estimate a more realistic error for the arm orientations in native $tRNA^{val}$. The rmsd of the experimentally measured RDCs for native $tRNA^{val}$ is 5.6 Hz (Table 2). The simulations show that if all the rmsd error in the experimental data arose from structural noise this would lead to an interarm angle uncertainty of more than 10°. However, for real data, part of the rmsd will arise from other factors besides structural noise (errors in measurement of RDCs, errors in estimates of D_a, R, or S). As noted above, these errors contribute less to uncertainty in the interarm angles; thus 10°, represents a reasonable estimate of the uncertainty in interarm angles for the experiments on native and unmodified $tRNA^{val}$ performed here.

Crystal structures of yeast $tRNA^{phe}$, yeast $tRNA^{asp}$, yeast initiator $tRNA^{fmet}$, and human $tRNA^{lys}$ show interarm angles ranging from 76 to 96° (*14*−*18*), and the results here indicate that the RDC measurements performed here would be able to distinguish between arm orientations for tRNAs with the largest and smallest angles. However, the more subtle differences in the domain orientation between structures could not be detected using only $^1H-^{15}N$ RDCs for the stem regions of tRNA.

Hydrogen Exchange and Dynamics for Native and Unmodified $tRNA^{val}$. The solvent exchange kinetics for imino and amino protons in nucleic acids are very sensitive to hydrogen bonding interactions, base pair opening, and fluctuations of the secondary and tertiary structures (*33*, *34*). Johnston et al. previously observed four very slowly exchanging imino protons for native yeast $tRNA^{phe}$ with half-lives on the order of minutes to days (*35*). Slowly exchanging imino protons in the D-stem and T-stem have also been observed for other native tRNAs (*E. coli* $tRNA^{fmet}$, $tRNA^{glu}$, and $tRNA^{trp}$; yeast $tRNA^{phe}$ and $tRNA^{asp}$; beef liver $tRNA^{trp}$; and *Thermus thermophilus* $tRNA^{ile}$); however, there are no analogous results for unmodified tRNAs (*35*−*37*, *54*). Deuterium exchange kinetics for native and unmodified *E. coli* $tRNA^{val}$ were measured here to better understand how modifications affect tRNA dynamics in solution. Unmodified $tRNA^{val}$ shows slowly exchanging imino protons in the D- and T-stem with exchange half-lives ranging from 3 to 73 min (Table 4). Although these half-lives are much shorter than that for the native $tRNA^{val}$ (T54/G24 has a half-life of 1500 min), the imino protons with the longest lifetimes in native $tRNA^{val}$ are also the most slowly exchanging in unmodified $tRNA^{val}$. For both the native and unmodified $tRNA^{val}$, the most slowly exchanging protons are involved in tertiary interactions in the D- and T-stems, suggesting that these unique tertiary interactions, particularly extensive stacking of the triples in the D-stem, contribute to this slow exchange (Figure 1). Results for the exchange times for the base triples in DNA support the idea that the additional

interaction from the third base in the triple contributes to the slow exchange. For example, Powell et al. observed that the G imino proton in a G-C-C$^+$ triple and the Watson−Crick T imino proton in an A-T-T triple have half-lives of 26 and 5.7 min, respectively (*55*). The DNA triplex experiments were carried out at pH 5.5 and 10 °C. Since a lower pH slows exchange, the results on DNA compare well with the data here for unmodified tRNA^{val} where the imino protons for residues G22 and G10 that are involved in C-G-G triples have half-lives of ∼3−5 min at pH 7.0 and 5 °C.

CONCLUSIONS

The data presented here represent the first comparison of the global structure and dynamics of native and unmodified free tRNA in solution. The vast majority (24 of 27) of the normalized imino ^{1}H−^{15}N RDCs in native and unmodified tRNA^{val} have similar values, which qualitatively shows that there are no significant differences in local or global structures of the helical arms between native and unmodified tRNA^{val}. Domain orientation techniques were next used to determine the bend and twist angles for the helical arms in these tRNAs. These data showed that within error of the calculations, both tRNAs have the same bend (∼101°) and twist (∼178°) angles. Thus, the solution NMR studies here demonstrate that the more easily produced unmodified tRNA^{val} represents a good model system for the global structure of native tRNA^{val}. A comparison of native and unmodified tRNA in crystal structures for native or unmodified tRNA^{gln} complexed with *E. coli* glutaminyl-tRNA synthetase is consistent with these results (*56*, *57*). The two tRNAs have essentially identical crystal structures, except for small differences in atomic positions related to the modifications.

In contrast to the structural data, comparison of the hydrogen exchange data shows significant differences between native and unmodified tRNA^{val}, where the half-lives for the most slowly exchanging imino protons decrease up to 20-fold in unmodified tRNA^{val}. Current models of hydrogen exchange in nucleic acids propose that exchange takes place only when the imino proton is exposed to solvent (*34*). Thus, the hydrogen bonds in the base pair (or triple) are broken, and the base pair must open for the imino proton to exchange with solvent. The large changes in imino proton exchange rates indicate that there are major differences in the dynamics of the secondary and/or tertiary structure between modified and unmodified tRNA^{val}. Since the open state of these slowly exchanging base pairs represents only a small percentage of the structures in solution, they do not contribute significantly to the RDC data. Therefore, the NMR studies here show that post-transcriptional modifications affect the exchange kinetics but not the local or global structures for the imino protons in the tRNAs. Previous studies have shown large differences in the melting temperatures of modified and unmodified tRNAs (*8*, *9*). Combined with the NMR data here, these data lead to a model in which the modifications primarily affect the thermodynamic stability and kinetics for hydrogen exchange but not the structure. Since thermophiles contain a higher percentage of modifications in their tRNA, and have higher melting temperatures (*12*), it is expected that, well below their growth temperature, thermophilic tRNA will have decreased dynamics and therefore slower exchange kinetics for their imino protons. This is not what has been observed in native *T. thermophilus* tRNA^{ile}, where the kinetics of the most slowly exchanging imino protons at 5 °C are actually faster than those of the most slowly exchanging imino protons in *E. coli* and yeast tRNAs (*35*−*37*, *54*). However, since these measurements were performed at low temperatures, they do not reflect the dynamics of these tRNAs under their normal growth conditions. The deuterium exchange rates are usually too fast to be measured by NMR at higher temperatures. Thus, other techniques, such as measurement of NMR relaxation times, are required to more directly compare the dynamics of mesophilic and thermophilic tRNAs. Recent studies on the dynamics of protein enzymes have indicated similar catalytic rates and local dynamics of mesophilic and thermophilic enzymes at their normal operating temperatures (*58*). It would be interesting to see if similar effects are observed for the dynamics of meso- and thermophilic RNAs.

The half-lives for exchange of imino protons in standard double-helical DNAs and RNAs are generally on the order of seconds (*34*, *59*, *60*), and much longer exchange times (greater than minutes) have only been observed in a few nucleic acids besides tRNAs. The most slowly exchanging imino protons that have been measured are in DNA G-quartets which can have half-lives longer than 2 weeks (*61*). Some DNA triplexes also have imino protons with long exchange times, but these only form at lower pH (which also slows the exchange process) (*55*). Thus, it is intriguing that we observed several very slowly exchanging imino protons in unmodified *E. coli* tRNA^{val}. These results show that post-transcriptional modifications are not required for the existence of slowly exchanging imino protons in RNAs. Given the growing number of biological functions that have been identified for RNAs, it will be very interesting to see how many of these functional RNAs also exhibit slowly exchanging imino protons. Some of these larger functional RNAs (i.e., group I and group II ribozymes, riboswitches, and RNase P) likely have more globular structures than tRNA and thus are good candidates for having slowly exchanging imino protons. If these larger RNAs show a significant number of slowly exchanging imino protons, then deuterium exchange could provide a valuable tool for probing RNA structure and dynamics, which is similar to how it is currently used in studies of protein structure and dynamics. We are currently performing NMR deuterium exchange experiments on other functional RNAs, to determine how commonly slowly exchanging imino protons are observed in larger RNAs.

ACKNOWLEDGMENT

We thank Helen Rechsteiner for help in synthesis of the some of the tRNA samples, Marella Canny for help with the deuterium exchange experiments, and Dr. Emilia Mollova for valuable discussions.

SUPPORTING INFORMATION AVAILABLE

Tables with detailed parameters from NMR experiments, the effect of varying magnitudes of the alignment tensor on domain orientation calculations, and figures illustrating the structural noise in the simulations and RDCs as a function of position in tRNA. This material is available free of charge via the Internet at http://pubs.acs.org.

REFERENCES

1. Bjork, G. R., Durand, J. M., Hagervall, T. G., Leipuviene, R., Lundgren, H. K., Nilsson, K., Chen, P., Qian, Q., and Urbonavicius, J. (1999) Transfer RNA modification: Influence on translational frameshifting and metabolism, *FEBS Lett. 452*, 47−51.
2. Crain, P. F., and McCloskey, J. A. (2003) http://medstat.med.utah.edu/RNAmods/, University of Utah, Salt Lake City, UT.
3. Hall, K. B., Sampson, J. R., Uhlenbeck, O. C., and Redfield, A. G. (1989) Structure of an unmodified tRNA molecule, *Biochemistry 28*, 5794−5801.
4. Arnez, J. G., and Moras, D. (1999) Transfer RNA, in *Oxford Handbook of Nucleic Acid Structure* (Neidle, S., Ed.) pp 603−651, Oxford University Press, New York.
5. Curran, J. F. (1998) Modified Nucleotides in Translation, in *Modification and Editing of RNA* (Grosjean, H., and Benne, R., Eds.) pp 493−516, ASM Press, Washington, DC.
6. Vacher, J., Grosjean, H., Houssier, C., and Buckingham, R. H. (1984) The effect of point mutations affecting *Escherichia coli* tryptophan tRNA on anticodon-anticodon interactions and on UGA suppression, *J. Mol. Biol. 177*, 329−342.
7. Chu, W. C., and Horowitz, J. (1989) ^{19}F NMR of 5-fluorouracil-substituted transfer RNA transcribed in vitro: Resonance assignment of fluorouracil-guanine base pairs, *Nucleic Acids Res. 17*, 7241−7252.
8. Sampson, J. R., and Uhlenbeck, O. C. (1988) Biochemical and physical characterization of an unmodified yeast phenylalanine transfer RNA transcribed in vitro, *Proc. Natl. Acad. Sci. U.S.A. 85*, 1033−1037.
9. Derrick, W. B., and Horowitz, J. (1993) Probing Structural Differences between Native and in-Vitro Transcribed *Escherichia coli* Valine Transfer RNA: Evidence for Stable Base Modification-Dependent Conformers, *Nucleic Acids Res. 21*, 4948−4953.
10. Serebrov, V., Vassilenko, K., Kholod, N., Gross, H. J., and Kisselev, L. (1998) Mg^{2+} binding and structural stability of mature and in vitro synthesized unmodified *Escherichia coli* tRNAPhe, *Nucleic Acids Res. 26*, 2723−2728.
11. Perret, V., Garcia, A., Puglisi, J., Grosjean, H., Ebel, J. P., Florentz, C., and Giege, R. (1990) Conformation in solution of yeast $tRNA^{Asp}$ transcripts deprived of modified nucleotides, *Biochimie 72*, 735−743.
12. Kowalak, J. A., Dalluge, J. J., McCloskey, J. A., and Stetter, K. O. (1994) The role of posttranscriptional modification in stabilization of transfer RNA from hyperthermophiles, *Biochemistry 33*, 7869−7876.
13. Yue, D., Kintanar, A., and Horowitz, J. (1994) Nucleoside modifications stabilize Mg^{2+} binding in *Escherichia coli* $tRNA^{Val}$: An imino proton NMR investigation, *Biochemistry 33*, 8905−8911.
14. Hingerty, B., Brown, R. S., and Jack, A. (1978) Further refinement of the structure of yeast tRNAPhe, *J. Mol. Biol. 124*, 523−534.
15. Westhof, E., Dumas, P., and Moras, D. (1985) Crystallographic refinement of yeast aspartic acid transfer RNA, *J. Mol. Biol. 184*, 119−145.
16. Basavappa, R., and Sigler, P. B. (1991) The 3 Å crystal structure of yeast initiator tRNA: Functional implications in initiator/elongator discrimination, *EMBO J. 10*, 3105−3111.
17. Woo, N. H., Roe, B. A., and Rich, A. (1980) Three-dimensional structure of *Escherichia coli* initiator $tRNA^{fMet}$, *Nature 286*, 346−351.
18. Benas, P., Bec, G., Keith, G., Marquet, R., Ehresmann, C., Ehresmann, B., and Dumas, P. (2000) The crystal structure of HIV reverse-transcription primer $tRNA^{Lys,3}$ shows a canonical anticodon loop, *RNA 6*, 1347−1355.
19. Friederich, M. W., and Hagerman, P. J. (1997) The angle between the anticodon and aminoacyl acceptor stems of yeast $tRNA^{Phe}$ is strongly modulated by magnesium ions, *Biochemistry 36*, 6090−6099.
20. Friederich, M. W., Vacano, E., and Hagerman, P. J. (1998) Global flexibility of tertiary structure in RNA: Yeast $tRNA^{Phe}$ as a model system, *Proc. Natl. Acad. Sci. U.S.A. 95*, 3572−3577.
21. Vermeulen, A., Zhou, H. J., and Pardi, A. (2000) Determining DNA Global Structure and DNA Bending by Application of NMR Residual Dipolar Couplings, *J. Am. Chem. Soc. 122*, 9638−9647.
22. Bothnerby, A. A., Dadok, J., Mishra, P. K., and Vanzijl, P. C. M. (1987) High-Field NMR Determination of Magnetic-Susceptibility Tensors and Angular-Correlation Factors of Halomethanes, *J. Am. Chem. Soc. 109*, 4180−4184.
23. Tolman, J. R., Flanagan, J. M., Kennedy, M. A., and Prestegard, J. H. (1995) Nuclear magnetic dipole interactions in field-oriented proteins: Information for structure determination in solution, *Proc. Natl. Acad. Sci. U.S.A. 92*, 9279−9283.
24. Tjandra, N., and Bax, A. (1997) Direct measurement of distances and angles in biomolecules by NMR in a dilute liquid crystalline medium, *Science 278*, 1111−1114.
25. Tjandra, N., Omichinski, J. G., Gronenborn, A. M., Clore, G. M., and Bax, A. (1997) Use of dipolar ^{1}H-^{15}N and ^{1}H-^{13}C couplings in the structure determination of magnetically oriented macromolecules in solution, *Nat. Struct. Biol. 4*, 732−738.
26. Fischer, M. W., Losonczi, J. A., Weaver, J. L., and Prestegard, J. H. (1999) Domain orientation and dynamics in multidomain proteins from residual dipolar couplings, *Biochemistry 38*, 9013−9022.
27. Skrynnikov, N. R., and Kay, L. E. (2000) Assessment of molecular structure using frame-independent orientational restraints derived from residual dipolar couplings, *J. Biomol. NMR 18*, 239−252.
28. Mollova, E. T., Hansen, M. R., and Pardi, A. (2000) Global structure of RNA determined with residual dipolar couplings, *J. Am. Chem. Soc. 122*, 11561−11562.
29. Bondensgaard, K., Mollova, E. T., and Pardi, A. (2002) The global conformation of the hammerhead ribozyme determined using residual dipolar couplings, *Biochemistry 41*, 11532−11542.
30. Tsui, V., Zhu, L., Huang, T. H., Wright, P. E., and Case, D. A. (2000) Assessment of zinc finger orientations by residual dipolar coupling constants, *J. Biomol. NMR 16*, 9−21.
31. Bewley, C. A. (2001) Rapid validation of the overall structure of an internal domain-swapped mutant of the anti-HIV protein cyanovirin-N using residual dipolar couplings, *J. Am. Chem. Soc. 123*, 1014−1015.
32. Sibille, N., Pardi, A., Simorre, J. P., and Blackledge, M. (2001) Refinement of local and long-range structural order in theophylline-binding RNA using ^{13}C−^{1}H residual dipolar couplings and restrained molecular dynamics, *J. Am. Chem. Soc. 123*, 12135−12146.
33. Englander, S. W., and Kallenbach, N. R. (1983) Hydrogen exchange and structural dynamics of proteins and nucleic acids, *Q. Rev. Biophys. 16*, 521−655.
34. Gueron, M., and Leroy, J. L. (1995) Studies of Base Pair Kinetics by NMR Measurement of Proton Exchange, *Methods Enzymol. 261*, 383−413.
35. Johnston, P. D., Figueroa, N., and Redfield, A. G. (1979) Real-time solvent exchange studies of the imino and amino protons of yeast phenylalanine transfer RNA by Fourier transform NMR, *Proc. Natl. Acad. Sci. U.S.A. 76*, 3130−3134.
36. Leroy, J. L., Bolo, N., Figueroa, N., Plateau, P., and Gueron, M. (1985) Internal Motions of Transfer RNA: A Study of Exchanging Protons by Magnetic Resonance, *J. Biomol. Struct. Dyn. 2*, 915−939.
37. Choi, B. S., and Redfield, A. G. (1995) Proton exchange and basepair kinetics of yeast $tRNA^{Phe}$ and $tRNA^{Asp1}$, *J. Biochem. 117*, 515−520.
38. Vermeulen, A. (2003) Determining Nucleic Acid Global Structure by Application of NMR Residual Dipolar Couplings, Ph.D. Thesis, University of Colorado, Boulder, CO.
39. Yue, D. (1994) Structure and Function of Unmodified *E. coli* Valine-tRNA, Ph.D. Thesis, Iowa State University, Ames, IA.
40. Ruckert, M., and Otting, G. (2000) Alignment of biological macromolecules in novel nonionic liquid crystalline media for NMR experiments, *J. Am. Chem. Soc. 122*, 7793−7797.
41. Hansen, M. R., Hanson, P., and Pardi, A. (2000) Filamentous bacteriophage for aligning RNA, DNA, and proteins for measurement of nuclear magnetic resonance dipolar coupling interactions, *Methods Enzymol. 317*, 220−240.
42. Plateau, P., and Gueron, M. (1982) Exchangeable Proton NMR without Base-Line Distortion, Using New Strong-Pulse Sequences, *J. Am. Chem. Soc. 104*, 7310−7311.
43. Wijmenga, S. S., Mooren, M. M. W., and Hilbers, C. W. (1993) NMR Studies of Nucleic Acids; From Spectrum to Structure, in *NMR of Macromolecules* (Roberts, G. C. K., Ed.) pp 217−288, Oxford University Press, Oxford, U.K.
44. Sklenár, V., and Bax, A. (1987) Two-dimensional Heteronuclear Chemical-Shift Correlation in Proteins at Natural Abundance ^{15}N and ^{13}C Levels, *J. Magn. Reson. 71*, 379−383.
45. Hare, D. R., Ribeiro, N. S., Wemmer, D. E., and Reid, B. R. (1985) Complete assignment of the imino protons of *Escherichia coli* valine transfer RNA: Two-dimensional NMR studies in water, *Biochemistry 24*, 4300−4306.

46. Cordier, F., Dingley, A. J., and Grzesiek, S. (1999) A doublet-separated sensitivity-enhanced HSQC for the determination of scalar and dipolar one-bond J-couplings, *J. Biomol. NMR 13*, 175−180.
47. Bax, A., Kontaxis, G., and Tjandra, N. (2001) Dipolar Couplings in Macromolecular Structure Determination, *Methods Enzymol. 339*, 127−174.
48. Brunger, A. T. (1992) *X-PLOR 3.1: A system for X-ray Crystallography and NMR*, Yale University Press, New Haven, CT.
49. McCallum, S. A., and Pardi, A. (2003) Refined Solution Structure of the Iron Responsive Element RNA Using Residual Dipolar Couplings, *J. Mol. Biol. 326*, 1037−1050.
50. Zweckstetter, M., and Bax, A. (2002) Evaluation of uncertainty in alignment tensors obtained from dipolar couplings, *J. Biomol. NMR 23*, 127−137.
51. Lavery, R., and Sklenar, H. (1989) Defining the Structure of Irregular Nucleic Acids: Conventions and Principles, *J. Biomol. Struct. Dyn. 6*, 655−667.
52. Mesleh, M. F., Veglia, G., DeSilva, T. M., Marassi, F. M., and Opella, S. J. (2002) Dipolar waves as NMR maps of protein structure, *J. Am. Chem. Soc. 124*, 4206−4207.
53. Walsh, J. D., Cabello-Villegas, J., and Wang, Y. X. (2004) Periodicity in residual dipolar couplings and nucleic acid structures, *J. Am. Chem. Soc. 126*, 1938−1939.
54. Figueroa, N., Keith, G., Leroy, J. L., Plateau, P., Roy, S., and Gueron, M. (1983) NMR study of slowly exchanging imino protons in yeast tRNA^{asp}, *Proc. Natl. Acad. Sci. U.S.A. 80*, 4330−4333.
55. Powell, S. W., Jiang, L., and Russu, I. M. (2001) Proton exchange and base pair opening in a DNA triple helix, *Biochemistry 40*, 11065−11072.
56. Rould, M. A., Perona, J. J., Soll, D., and Steitz, T. A. (1989) Structure of *E. coli* glutaminyl-tRNA synthetase complexed with tRNA^{Gln} and ATP at 2.8 Å resolution, *Science 246*, 1135−1142.
57. Arnez, J. G., and Steitz, T. A. (1994) Crystal structure of unmodified tRNA^{Gln} complexed with glutaminyl-tRNA synthetase and ATP suggests a possible role for pseudo-uridines in stabilization of RNA structure, *Biochemistry 33*, 7560−7567.
58. Wolf-Watz, M., Thai, V., Henzler-Wildman, K., Hadjipavlou, G., Eisenmesser, E. Z., and Kern, D. (2004) Linkage between dynamics and catalysis in a thermophilic-mesophilic enzyme pair, *Nat. Struct. Mol. Biol. 11*, 945−949.
59. Snoussi, K., and Leroy, J. L. (2001) Imino proton exchange and base-pair kinetics in RNA duplexes, *Biochemistry 40*, 8898−8904.
60. Pardi, A., and Tinoco, I. (1982) Kinetics for exchange of imino protons in deoxyribonucleic acid, ribonucleic acid, and hybrid oligonucleotide helices, *Biochemistry 21*, 4686−4693.
61. Smith, F. W., and Feigon, J. (1992) Quadruplex structure of *Oxytricha* telomeric DNA oligonucleotides, *Nature 356*, 164−168.

BI0473399